IET Renewable Power Generation

Special Issue Call for Papers

Be Seen. Be Cited.
Submit your work to a new IET special issue

Connect with researchers and experts in your field and share knowledge.

Be part of the latest research trends, faster.

Read more

The Institution of Engineering and Technology

Received: 10 February 2021 | Revised: 21 June 2021 | Accepted: 1 July 2021

IET Renewable Power Generation

DOI: 10.1049/rpg2.12242

The Institution of Engineering and Technology WILEY

ORIGINAL RESEARCH PAPER

Wave energy converter platform stabilisation and mooring load reduction through power take-off control

A.J. Hillis[1] | C.R.P. Courtney[1] | A. Brask[2]

[1] Department of Mechanical Engineering, University of Bath, Bath, UK

[2] Marine Power Systems Ltd, Ethos Building, Kings Road, Swansea, UK

Correspondence
A.J. Hillis, Department of Mechanical Engineering, University of Bath, Bath BA2 7AY, UK.
Email: a.j.hillis@bath.ac.uk

Abstract

Mooring systems are a significant capital cost of a floating wave energy converter and their premature failure negatively impacts operational costs. Excessive peak loads and accumulated fatigue damage can lead to failure, so these factors are cost drivers in wave energy converter design. Here, the potential to reduce platform motion and mooring loads through modification of the power take-off (PTO) control are investigated. An approximate velocity tracking control strategy is implemented with a linear quadratic regulator design method using differential weighting of system states. It is demonstrated that the controller can be tuned to capture similar mean power to an optimally tuned, passively damped system while significantly reducing mooring line cyclic loading. The relative accumulated fatigue damage in the mooring lines in a high energy sea-state is found to be reduced by between 43% and 92% as a result of using the approximate velocity tracking control strategy.

1 | INTRODUCTION

The overall cost of a wave energy converter (WEC) is driven by many factors. The mooring system is a significant capital cost of a floating WEC [1], and its premature failure would negatively impact operational costs. The mooring system must function for the design lifetime of the WEC installation, which could be 20 years. During this time, it will be subject to high wave loading relative to other types of moored structures since a WEC could be deliberately located in an energetic location with high wave power resource. The moorings must also achieve the function of station-keeping to minimise the impact of gross motion of the WEC on power capture and structural loading. The mooring cost is directly related to station-keeping in the most severe design condition, and to accommodating fatigue loading over its lifetime [2]. For many WEC designs, therefore, the peak and fatigue mooring forces are a cost-driver so it is important to investigate methods for their reduction.

Studies have investigated mooring load reductions in high loading situations through direct actuation or damping of the mooring system, e.g. [3]. While this may be effective, the introduction of additional components bring associated cost and reliability impacts. The example WEC studied here uses a taut mooring system. Mooring loads are determined by the motion of the parts of the WEC structure connected to the moorings. The mooring loads are also strongly coupled to power take-off (PTO) input forces, which react against the moored structure. This raises the possibility of using the PTO control strategy to influence the mooring loads, not only to reduce peak loads but also to reduce the cyclic loading component and therefore reduce accumulated fatigue damage. Most WEC control studies focus on maximising energy capture in the PTO as a means of improving cost efficiency. In general, a control strategy provides a means of balancing multiple competing requirements. The focus of the present study is the trade-off between captured power and the coupled considerations of mooring line loading and platform stability. Stability is particularly important for the emerging combined wind/wave converters e.g. [4, 5] and the possibility of using the WEC to improve stability has been studied in [6].

Many control architectures would be suitable for this objective, and there are advantages and disadvantages to the various approaches. Model-predictive control (MPC) and pseudospectral control, for example, can minimise a weighted cost function incorporating energy capture and any other relationship between modelled system states whilst simultaneously imposing constraints on them. Thus, one could readily maximise energy capture while constraining the states associated with mooring

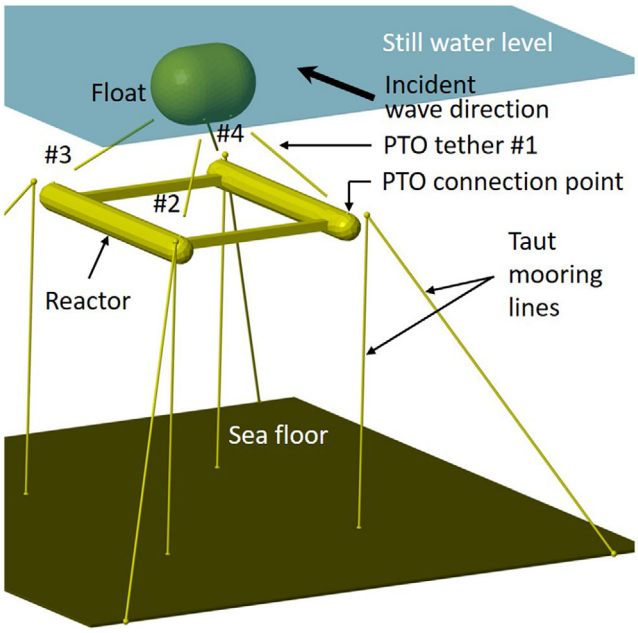

FIGURE 1 Simplified geometry and mooring in WEC-Sim (reproduced from [10])

loads. The disadvantages are the requirement for predicting the wave excitation force, sensitivity to modelling errors and computational effort for realistic prediction horizons. A detailed overview and comparison of these methods can be found in [7]. An alternative is to use the approximate velocity tracking (AVT) controller originally proposed in [8] and used in [9]. This has the advantages of computational simplicity and robustness against model uncertainty. As for MPC and many other WEC control strategies, the unmeasurable wave excitation force must be estimated on-line. Unlike MPC, forward prediction of the excitation force is not required. The AVT controller is modified to include an intuitive method to balance power capture with mooring loads. Constraints can still be applied to system states, but in a far more limited manner compared to MPC/pseudo-spectral control.

The remainder of the paper is organised as follows. Descriptions of the WEC multi-body simulation model and its linearised equivalent are provided in Section 2. The control strategy is described in Section 3. Simulation results comparing a passive benchmark system performance against the actively controlled system in irregular waves are presented and discussed in Section 4. Finally, conclusions are drawn from the study in Section 5.

2 | THE WAVESUB WEC

2.1 | General overview

The WEC under consideration in this study is a previous generation of WaveSub which is under development by Marine Power Systems Ltd. Figure 1 shows a simplified representation of the system geometry which is used in the multi-body simulation described in the following section.

It is a submerged point absorber designed to convert wave power through motion of a float in the surge and heave directions. Power is converted through four taut tethers connected to PTOs mounted at the four corners of a reactor. In one possible physical embodiment the PTO would be geared rotary generators connected to the shafts of drums around which the PTO tethers are wrapped. The PTO tethers are also connected to passive springs with stiffnesses tuned to the prevailing wave conditions. The reactor is moored to the seabed by 8 taut compliant mooring lines (four vertical and four diagonal). Preload is applied to PTO and mooring lines to balance the buoyancy forces of the two bodies.

2.2 | Multi-body simulation model

WaveSub is simulated in the time-domain using the WEC-Sim modelling environment [11]. The formulation of the forces acting on a WEC are well documented in the literature, so are summarised here.

The dynamics of a general single submerged WEC body are governed by:

$$\mathbf{M}\ddot{\mathbf{x}}(t) = \mathbf{f}_{\mathrm{e}}(t) + \mathbf{f}_{\mathrm{r}}(t) + \mathbf{f}_{\mathrm{hs}}(t) + \mathbf{f}_{\mathrm{v}}(t) + \mathbf{f}_{\mathrm{PTO}}(t) + \mathbf{f}_{\mathrm{M}}(t) \quad (1)$$

where $\mathbf{M} \in \mathbb{R}^{6\times 6}$ is the mass matrix and $\mathbf{x} = [x\ y\ z\ \theta_x\ \theta_y\ \theta_z]^T$ is the 6-DOF state vector with surge, sway and heave displacements, and roll, pitch and yaw rotations. The 6-DOF force vectors are defined as follows. $\mathbf{f}_{\mathrm{e}}$ is the wave excitation force, $\mathbf{f}_{\mathrm{r}}$ is the radiation damping force, $\mathbf{f}_{\mathrm{hs}}$ is the hydrostatic restoring force, and $\mathbf{f}_{\mathrm{v}}$ is a nonlinear viscous damping term which is commonly neglected. The PTO and moorings provide the mechanical forces $\mathbf{f}_{\mathrm{PTO}}$ and $\mathbf{f}_{\mathrm{M}}$, respectively. The excitation and radiation forces are calculated using hydrodynamic coefficients computed by the NEMOH boundary element method (BEM) solver [12].

The excitation force is given by

$$\mathbf{f}_{\mathrm{e}} = \mathbb{R}\left[\sum_{i=1}^{N} \sqrt{2\mathbf{S}(\omega_i)\Delta\omega_i}\mathbf{H}_{\mathrm{e}}(\omega_i)e^{j(\omega_i t+\phi_i)}\right] \quad (2)$$

where $\mathbf{H}_{\mathrm{e}}(\omega)$ and $\mathbf{S}(\omega)$ are the frequency-dependent excitation force frequency response function (FRF) and wave spectrum, respectively. N is the number of frequencies included in the spectra and ϕ_i is the random phase of the ith frequency component. The excitation FRFs for the reactor and float are presented in Figure 2.

The radiation force is given by [13]

$$\mathbf{f}_{\mathrm{r}}(t) = -\mathbf{M}_{\mathrm{a}}(\infty)\ddot{\mathbf{x}} - \int_0^t \mathbf{K}_{\mathrm{r}}(t-\tau)\dot{\mathbf{x}}(\tau)\mathrm{d}\tau \quad (3)$$

where $\mathbf{M}_{\mathrm{a}}(\infty) \in \mathbb{R}^{6\times 6}$ is the infinite frequency added mass matrix and $\mathbf{K}_{\mathrm{r}}$ is the radiation impulse response function (IRF)

from the BEM solution. The added mass and radiation damping coefficients for the reactor and float are shown in Figures 3 and 4, respectively.

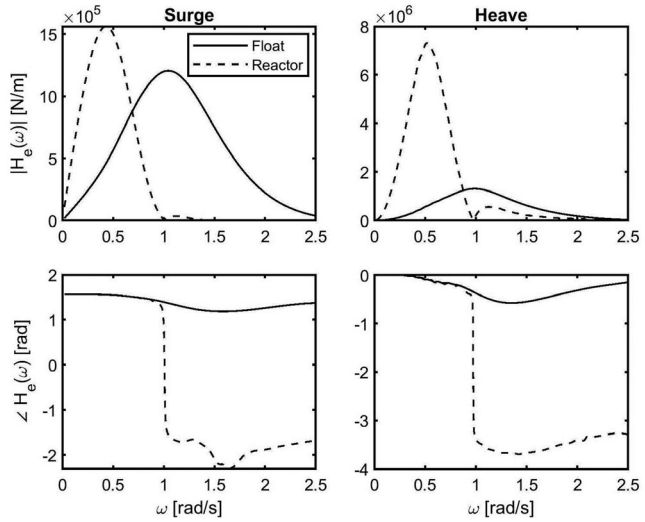

FIGURE 2 Excitation FRFs of the reactor and float

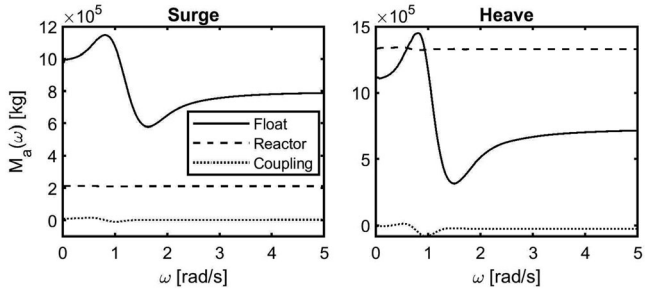

FIGURE 3 Added mass coefficients of the reactor and float

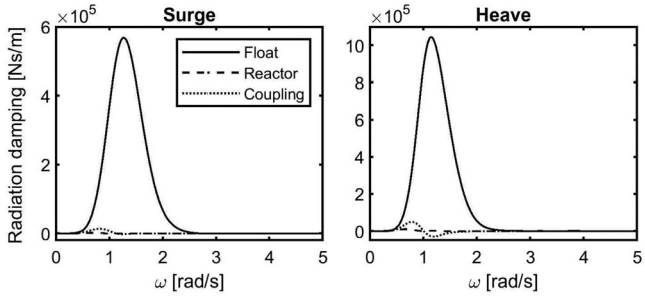

FIGURE 4 Radiation damping coefficients of the reactor and float

$\mathbf{F}_{\mathrm{hs}}(t)$ is constant for a fully submerged body. In the heave direction it is given by

$$F_{\mathrm{hs}}(t) = -\rho g V \tag{4}$$

where ρ is the water density, g is the acceleration due to gravity and V is the body volume.

The PTO force is given by

$$\mathbf{f}_{\mathrm{PTO}} = \mathbf{u}_{\mathrm{C}} + \mathbf{K}_{\mathrm{PTO}}(\mathbf{x}_{\mathrm{F}} - \mathbf{x}_{\mathrm{R}}) \tag{5}$$

where $\mathbf{u}_{\mathrm{C}}$ is the control force in the Cartesian frame and $\mathbf{K}_{\mathrm{PTO}} \in \mathbb{R}^{6\times6}$ is the PTO spring stiffness matrix. The subscripts R and F refer to the reactor and float, respectively. Due to large float motions in operation, $\mathbf{K}_{\mathrm{PTO}}$ is not constant [10]. This is also true for the mooring system, but the reactor motion is much smaller than the float motion.

The mooring force is given by

$$\mathbf{f}_{\mathrm{M}} = \mathbf{K}_{\mathrm{M}}\mathbf{x}_{\mathrm{R}} + \mathbf{C}_{\mathrm{M}}\dot{\mathbf{x}}_{\mathrm{R}} \tag{6}$$

where $\mathbf{K}_{\mathrm{M}} \in \mathbb{R}^{6\times6}$ and $\mathbf{C}_{\mathrm{M}} \in \mathbb{R}^{6\times6}$ are the mooring stiffness and damping matrices. The damping represents forces due to internal abrasion of mooring rope fibres.

For the coupled two-body system here, the equation of motion is given by

$$\begin{bmatrix}\mathbf{M}_{\mathrm{R}} & \mathbf{0}\\ \mathbf{0} & \mathbf{M}_{\mathrm{F}}\end{bmatrix}\begin{bmatrix}\ddot{\mathbf{x}}_{\mathrm{R}}\\ \ddot{\mathbf{x}}_{\mathrm{F}}\end{bmatrix} = \begin{bmatrix}\mathbf{f}_{\mathrm{eR}}\\ \mathbf{f}_{\mathrm{eF}}\end{bmatrix} + \begin{bmatrix}\mathbf{f}_{\mathrm{rR}} + \mathbf{f}_{\mathrm{rR:F}}\\ \mathbf{f}_{\mathrm{rF}} + \mathbf{f}_{\mathrm{rF:R}}\end{bmatrix} + \begin{bmatrix}\mathbf{f}_{\mathrm{hsR}}\\ \mathbf{f}_{\mathrm{hsF}}\end{bmatrix} + \begin{bmatrix}\mathbf{f}_{\mathrm{vR}}\\ \mathbf{f}_{\mathrm{vF}}\end{bmatrix} + \begin{bmatrix}\mathbf{f}_{\mathrm{PTO}}\\ -\mathbf{f}_{\mathrm{PTO}}\end{bmatrix} + \begin{bmatrix}\mathbf{f}_{\mathrm{M}}\\ \mathbf{0}\end{bmatrix} \tag{7}$$

where $\{\mathbf{f}_{\mathrm{rR:F}}, \mathbf{f}_{\mathrm{rF:R}}\}$ are the radiation force interactions between the two bodies. The main numerical model properties are summarised in Table 1. It should be noted that the PTO spring stiffness value is variable so the system may be tuned to resonate with the dominant wave energy period (T_{e}). The mooring stiffness is fixed for all sea-states.

TABLE 1 Dimensions of the full scale numerical model

Property	Value	Unit
Float diameter	12	m
Float mass	1.2×10^6	kg
Reactor length	52	m
Reactor width	50	m
Reactor height	5	m
Reactor mass	1.1×10^6	kg
PTO spring stiffness:		
$T_{\mathrm{e}} = 6$ s:	1.20	MN/m
$T_{\mathrm{e}} = 10$ s:	0.50	MN/m
$T_{\mathrm{e}} = 16$ s:	0.25	MN/m
Mooring line stiffness	15	MN/m
Water depth	75	m
Submergence (to top of float)	2	m

2.3 | Linearised dynamic system model

Most multi-variable control strategies require a linearised state-space model of the system for their formulation. The WEC under consideration here has previously been described in [10], where the reactor was assumed to be fixed by a taut mooring system. Here we are interested in exploring the effect of the control system on the reactor and mooring lines so the state-space model must be extended to include these elements. The new extended state vector is given by $\tilde{\mathbf{x}}(t) = [\mathbf{x}_R \;\; \mathbf{x}_F \;\; \dot{\mathbf{x}}_R \;\; \dot{\mathbf{x}}_F \;\; \mathbf{p}_{rR} \;\; \mathbf{p}_{rF}]^T$, where $\{\mathbf{p}_{rR}, \mathbf{p}_{rF}\}$ are vectors of auxiliary states of 4th order state-space approximations of the radiation impulse response functions of the reactor and float described by

$$\begin{aligned} \dot{\mathbf{p}}_{rR}(t) &= \mathbf{A}_{rR}\mathbf{p}_{rR}(t) + \mathbf{B}_{rR}\dot{\mathbf{x}}_R(t) \\ \int_0^t \mathbf{K}_{rR}(t-\tau)\dot{\mathbf{x}}_R(\tau)\mathrm{d}\tau &\approx \mathbf{C}_{rR}\mathbf{p}_{rR}(t) \\ \dot{\mathbf{p}}_{rF}(t) &= \mathbf{A}_{rF}\mathbf{p}_{rF}(t) + \mathbf{B}_{rF}\dot{\mathbf{x}}_F(t) \\ \int_0^t \mathbf{K}_{rF}(t-\tau)\dot{\mathbf{x}}_F(\tau)\mathrm{d}\tau &\approx \mathbf{C}_{rF}\mathbf{p}_{rF}(t) \end{aligned} \tag{8}$$

The matrices $\{\mathbf{A}_r, \mathbf{B}_r, \mathbf{C}_r\}$ are computed to approximate radiation impulse response functions $\mathbf{K}_{rR}(t)$ and $\mathbf{K}_{rF}(t)$ for the reactor and float. The radiation force model has four states for each Cartesian DOF so, maintaining generality by calculating for all six DOFs, we have twenty-four radiation states for each body. This can be reduced if body motion does not occur in some axes or if the body is circular about an axis of rotation.

Neglecting the time-dependency notation for clarity, and neglecting radiation force interaction between the two bodies (Figures 3 and 4 show these to be small), the WEC dynamics can be represented by the state-space system

$$\begin{aligned} \dot{\tilde{\mathbf{x}}} &= \mathbf{A}\tilde{\mathbf{x}} + \mathbf{B}[\mathbf{u} \;\; \mathbf{f}_{eR} \;\; \mathbf{f}_{eF}]^T \\ \mathbf{y} &= \mathbf{C}\tilde{\mathbf{x}} \end{aligned} \tag{9}$$

The system matrices are given in Equation (10), where $\mathbf{M}_\infty \in \mathbb{R}^{6\times6}$ is the sum of the body mass matrix and its infinite added mass matrix (obtained from the BEM solution), $\mathbf{B}_v \in \mathbb{R}^{6\times6}$ is a linear viscous damping matrix empirically tuned to experimental data [14], and $\{\mathbf{K}_M, \mathbf{K}_{PTO}\} \in \mathbb{R}^{6\times6}$ are the linearised stiffness matrices for the mooring and PTO lines, respectively (see [15]). These include pretension and spring stiffness terms and take the form

$$\begin{bmatrix} k_{xx} & 0 & 0 & 0 & k_{x,\theta_y} & 0 \\ 0 & k_{yy} & 0 & k_{y,\theta_x} & 0 & 0 \\ 0 & 0 & k_{zz} & 0 & 0 & 0 \\ 0 & k_{y,\theta_x} & 0 & k_{\theta_x,\theta_x} & 0 & 0 \\ k_{x,\theta_y} & 0 & 0 & 0 & k_{\theta_y,\theta_y} & 0 \\ 0 & 0 & 0 & 0 & 0 & k_{\theta_z,\theta_z} \end{bmatrix} \tag{11}$$

$\mathbf{J}_{PTO}^{-T} \in \mathbb{R}^{4\times6}$ is the inverse of the transposed kinematic Jacobian matrix used to map float forces and velocities between Cartesian and PTO line space [9]. It is given by

$$\mathbf{J}_{PTO}^{-1} = \begin{bmatrix} \mathbf{e}_{PTO,1}^{\mathbf{T}} & \left(\mathbf{F}_{PTO,1} \times \mathbf{e}_{PTO,1}\right)^T \\ \vdots & \vdots \\ \mathbf{e}_{PTO,4}^{T} & \left(\mathbf{F}_{PTO,4} \times \mathbf{e}_{PTO,4}\right)^T \end{bmatrix} \tag{12}$$

$$\mathbf{A} \in \mathbb{R}^{72\times72} = \begin{bmatrix} \mathbf{0} & \mathbf{0} & \mathbf{I} & \mathbf{0} & \mathbf{0} & \mathbf{0} \\ \mathbf{0} & \mathbf{0} & \mathbf{0} & \mathbf{I} & \mathbf{0} & \mathbf{0} \\ -\mathbf{M}_{\infty R}^{-1}(\mathbf{K}_M + \mathbf{K}_{PTO}) & \mathbf{M}_{\infty R}^{-1}\mathbf{K}_{PTO} & -\mathbf{M}_{\infty R}^{-1}(\mathbf{B}_{vR} + \mathbf{B}_{vF}) & \mathbf{M}_{\infty R}^{-1}\mathbf{B}_{vF} & -\mathbf{M}_{\infty R}^{-1}\mathbf{C}_{rR} & \mathbf{0} \\ \mathbf{M}_{\infty F}^{-1}\mathbf{K}_{PTO} & -\mathbf{M}_{\infty F}^{-1}\mathbf{K}_{PTO} & \mathbf{M}_{\infty F}^{-1}\mathbf{B}_{vF} & -\mathbf{M}_{\infty F}^{-1}\mathbf{B}_{vF} & \mathbf{0} & -\mathbf{M}_{\infty F}^{-1}\mathbf{C}_{rF} \\ \mathbf{0} & \mathbf{0} & \mathbf{B}_{rR} & \mathbf{0} & \mathbf{A}_{rR} & \mathbf{0} \\ \mathbf{0} & \mathbf{0} & \mathbf{0} & \mathbf{B}_{rF} & \mathbf{0} & \mathbf{A}_{rF} \end{bmatrix} \tag{10}$$

$$\mathbf{B} \in \mathbb{R}^{72\times16} = \begin{bmatrix} \mathbf{0} & \mathbf{0} & \mathbf{0} \\ \mathbf{0} & \mathbf{0} & \mathbf{0} \\ -\mathbf{M}_{\infty R}^{-1}\mathbf{J}_{PTO}^{-T} & \mathbf{M}_{\infty R} & \mathbf{0} \\ \mathbf{M}_{\infty F}^{-1}\mathbf{J}_{PTO}^{-T} & \mathbf{0} & \mathbf{M}_{\infty F} \\ \mathbf{0} & \mathbf{0} & \mathbf{0} \\ \mathbf{0} & \mathbf{0} & \mathbf{0} \end{bmatrix} \quad \mathbf{C} \in \mathbb{R}^{12\times72} = \begin{bmatrix} \mathbf{I} & \mathbf{0} & \mathbf{0} & \mathbf{0} & \mathbf{0} & \mathbf{0} \\ \mathbf{0} & \mathbf{0} & \mathbf{0} & \mathbf{I} & \mathbf{0} & \mathbf{0} \end{bmatrix}$$

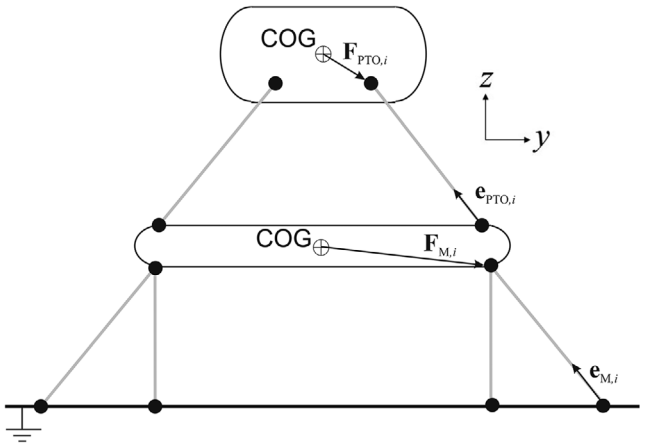

FIGURE 5 Illustration of WEC kinematics

With reference to Figure 5, $\mathbf{F}_{\mathrm{PTO},i}$ is the float connection point coordinate vector relative to the float centre of gravity and $\mathbf{e}_{\mathrm{PTO},i}$ is the unit vector along the direction of the ith PTO tether in the nominal WEC position.

We can also define a similar transform for the mooring system as

$$\mathbf{J}_{\mathrm{M}}^{-1} \in \mathbb{R}^{6\times 8} = \begin{bmatrix} \mathbf{e}_{\mathrm{M},1}^{\mathbf{T}} & \left(\mathbf{F}_{\mathrm{M},1} \times \mathbf{e}_{\mathrm{M},1}\right)^{T} \\ \vdots & \vdots \\ \mathbf{e}_{\mathrm{M},8}^{T} & \left(\mathbf{F}_{\mathrm{M},8} \times \mathbf{e}_{\mathrm{M},8}\right)^{T} \end{bmatrix} \tag{13}$$

The system input is a vector comprising the 4-DOF PTO control force $\mathbf{u}$ and $\{\mathbf{f}_{\mathrm{eR}}, \mathbf{f}_{\mathrm{eF}}\}$, which are the 6-DOF wave excitation force vectors acting on the reactor and float calculated using BEM-derived frequency-dependent excitation coefficients as shown in Equation (2) [16]. The system output is $[\mathbf{x}_{\mathrm{R}} \;\; \dot{\mathbf{x}}_{\mathrm{F}}]^{T}$.

Figure 6 compares the time-domain responses of the WEC-Sim and state-space approximation models for three irregular wave inputs characterised by Pierson–Moskowitz (PM) spectra with significant wave heights of $\{1, 3, 6\}$ m and energy periods of $\{6, 10, 16\}$ s, respectively. Excellent agreement is seen, with errors increasing in larger sea-states due to larger motion of the float inducing greater nonlinearity in the PTO stiffness. Using a standard normalised mean squared error goodness-of-fit measure between two vectors $\mathbf{x}_1, \mathbf{x}_2$,

$$\mathrm{GOF} = 1 - \frac{\|\mathbf{x}_1 - \mathbf{x}_2\|^2}{\|\mathbf{x}_1 - \mathrm{mean}(\mathbf{x}_1)\|^2} \tag{14}$$

where $\|$ denotes the Euclidean norm of a vector, we obtain maximum and minimum GOF values of 0.92 and 0.76, respectively, for the complete (700 s duration) datasets.

3 | OPTIMAL CONTROL STRATEGY

The control strategy presented here is an evolution of the AVT controller used in [9] and originally proposed in [8]. An optimal velocity trajectory for the float is computed in real-time and the PTO manipulated to force the float to track this trajectory. Here we assume head-on waves to be applied, so motion only occurs in the surge, heave and pitch directions. Pitch motion is uncontrollable since, in the nominal position, the PTO tethers point to the float COG. Therefore, we only need to control the float surge and heave velocities and the model/controller order could be reduced. We choose to preserve the order for the sake of generality since, for off-axis waves, action may be required in all controllable DOFs.

The overall control strategy is illustrated in Figure 7. The vector of Cartesian float velocity reference signals is given by

$$\dot{\mathbf{x}}_{\mathrm{refF}}(t) = \mathbf{G}^{-1}(t)\hat{\mathbf{f}}_{\mathrm{eF}}(t) = 0.5(|\mathbf{G}_{\mathrm{rF}}(\hat{\omega})| + \mathbf{B}_{\mathrm{vF}})^{-1}\hat{\mathbf{f}}_{\mathrm{eF}}(t) \tag{15}$$

where $|\mathbf{G}_{\mathrm{rF}}(\hat{\omega})|^{-1}$ is the inverse of a time-varying matrix of the instantaneous amplitudes of the float radiation damping models at the current estimated dominant excitation frequency $\hat{\omega}$. $\hat{\mathbf{f}}_{\mathrm{e}}(t)$ is the estimate of the float excitation force $\mathbf{f}_{\mathrm{e}}(t)$, which is assumed to be a narrow band harmonic process of the form [8]

$$\mathbf{f}_{\mathrm{e}}(t) = \mathbf{\Lambda}\cos(\boldsymbol{\omega} t + \boldsymbol{\phi}) \tag{16}$$

The estimation of $\mathbf{f}_{\mathrm{e}}(t)$ and the dominant amplitude $\hat{\mathbf{\Lambda}}$ and frequency $\hat{\boldsymbol{\omega}}$ of the excitation force may be achieved using an extended Kalman filter (EKF) as described in [9]. Position constraints are incorporated as a velocity constraint under the narrow band assumption so the velocity reference gain has an upper bound given by $\bar{\mathbf{G}}^{-1} = \hat{\boldsymbol{\omega}}.\bar{\mathbf{x}}./\hat{\mathbf{\Lambda}}$ where $\{.\}$ denotes elementwise multiplication or division and $\bar{\{\}}$ is the maximum permissible value of a quantity. Thus, a real-time variable gain on the velocity reference may be expressed as

$$\mathbf{G}^{-1}(t) = 0.5(|\mathbf{G}_{\mathrm{rF}}| + \mathbf{B}_{\mathrm{vF}})^{-1} \tag{17}$$

with the limit $\mathbf{G}^{-1} \leq \bar{\mathbf{G}}^{-1}$. Velocity reference tracking is achieved using LQR feedback under the assumption all states may be measured or accurately estimated. In [9] the primary objective was to maximise power capture, however the approach provides an intuitive means of balancing this with other operational considerations. Here we are specifically concerned with regulating reactor motion and reducing mooring loads via the PTO control. The state regulating gain matrix $\mathbf{K} \in \mathbb{R}^{4\times 72}$ is obtained from minimising the cost function

$$J(\mathbf{u}) = \int_0^{\infty} \left(\mathbf{y}^T\mathbf{Q}\mathbf{y} + \mathbf{u}^T\mathbf{R}\mathbf{u}\right)\mathrm{d}t \tag{17}$$

The resulting state feedback gain is

$$\mathbf{K} = \mathbf{R}^{-1}\mathbf{B}^T\mathbf{P} \tag{18}$$

where $\mathbf{P}$ is the solution to the algebraic Riccati equation

$$\mathbf{A}^T\mathbf{P} + \mathbf{P}\mathbf{A} - \mathbf{P}\mathbf{B}\mathbf{R}^{-1}\mathbf{B}^T\mathbf{P} + \mathbf{Q} = 0 \tag{19}$$

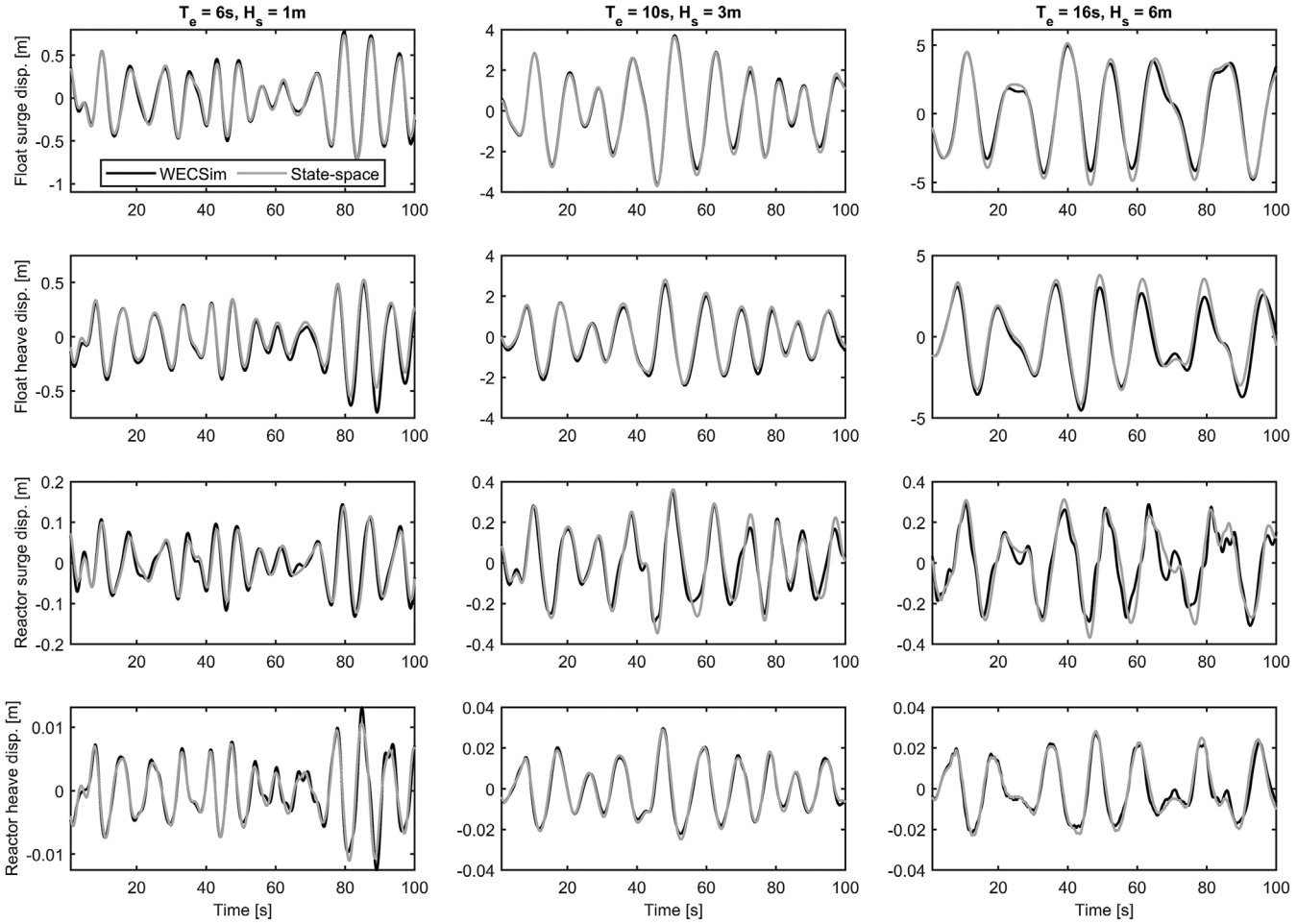

FIGURE 6 Comparison of irregular wave response of multi-body and linearised simulation models

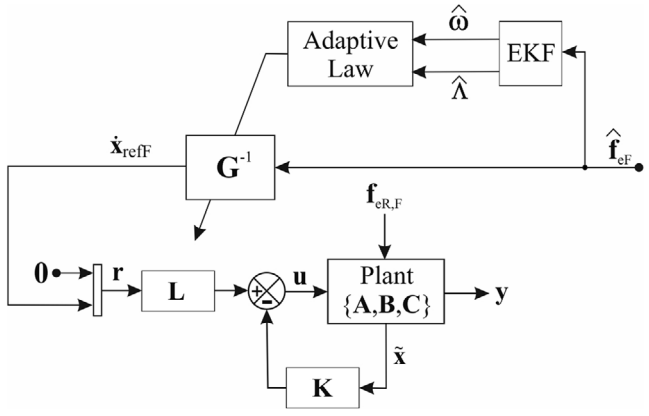

FIGURE 7 Illustration of AVT control strategy with LQR velocity tracking (adapted from [8])

Tracking of the float velocity is achieved using the compensator gain $\mathbf{L} \in \mathbb{R}^{4\times12}$, which is defined as

$$\mathbf{L} = [\mathbf{K}\ \mathbf{I}]\begin{bmatrix}\mathbf{A} & \mathbf{B}\\ \mathbf{C} & \mathbf{0}\end{bmatrix}^{-1}\begin{bmatrix}\mathbf{0}\\ \mathbf{I}\end{bmatrix} \tag{20}$$

The weighting matrices $\mathbf{Q} \in \mathbb{R}^{12\times12}$ and $\mathbf{R} \in \mathbb{R}^{4\times4}$ are defined as

$$\mathbf{Q} = \mathbf{C}^{\mathbf{T}}\begin{bmatrix}\bar{\mathbf{Q}} & \mathbf{0}\\ \mathbf{0} & \lambda\bar{\mathbf{Q}}\end{bmatrix}\mathbf{C} \quad \mathbf{R} = \rho\mathbf{I} \tag{21}$$

with λ tuned to balance reactor motion regulation with float velocity tracking, and ρ tuned to balance control effort. $\bar{\mathbf{Q}}$ is the auxiliary output error weighting matrix given by

$$\bar{\mathbf{Q}} = \frac{\bar{T}}{\bar{v}^2}\begin{bmatrix}|\mathrm{diag}([\mathbf{e}_{\mathrm{PTO}}])| & \mathbf{0}^{3\times3}\\ \mathbf{0}^{3\times3} & r.|\mathrm{diag}(\mathbf{F}_{\mathrm{PTO}}\times\mathbf{e}_{\mathrm{PTO}})|\end{bmatrix} \tag{22}$$

where T and v are the PTO tether tension and velocity respectively, and r is the radius of the float. $\{\mathbf{F}_{\mathrm{PTO}}, \mathbf{e}_{\mathrm{PTO}}\}$ are float and PTO line direction vectors as defined in Figure 5. The WEC has x–y symmetry so any of the four PTO lines can be used. This tuning method yields a good distribution of state penalties aiding both the solution of the LQR problem and the performance of the resulting feedback controller. The PTO control force

vector is given by

$$\mathbf{u} = \mathbf{L}\mathbf{r} - \mathbf{K}\tilde{\mathbf{x}} \tag{23}$$

where $\mathbf{r} = [\mathbf{0} \;\; \dot{\mathbf{x}}_{\text{refF}}]^T$ is the reference signal. It is necessary to avoid the PTO tethers becoming slack so a dynamic saturation constraint is imposed on $\mathbf{u}$, such that $\Delta\mathbf{u} \leq \mathbf{T}$, where $\Delta\mathbf{u}$ is the change in control force from the current time step and $\mathbf{T}$ is the vector of measured tether tensions.

4 | SIMULATION RESULTS

Simulations were conducted for three irregular wave inputs characterised by PM spectra with significant wave heights of $\{1, 3, 6\}$ m and energy periods of $\{6, 10, 16\}$ s, respectively. The spectra are displayed in Figure 8. Each case was simulated for 700 s using a fixed-step 4th order Runge–Kutta solver with step size 0.06 s. The instantaneous frequency and amplitude of the excitation force are estimated from the excitation force, which is assumed to be known precisely, but could readily be estimated as described in [9].

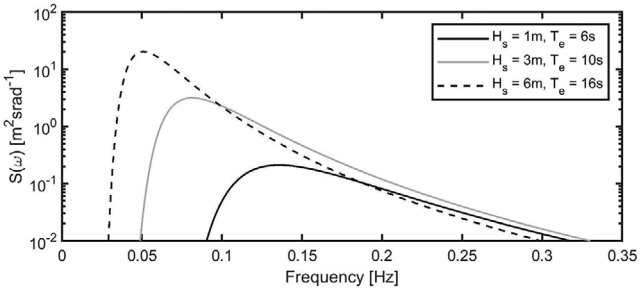

FIGURE 8 PM spectra of simulated sea-states

4.1 | Effect of control tuning on performance

Adjusting the ratio of the state penalty matrices by varying λ changes the balance of captured power and reactor motion (and therefore mooring line forces). Figure 9 shows the variation of mean captured power, peak mooring force and peak reactor displacement over 700 s simulations as λ is varied while keeping $\bar{\mathbf{Q}}$ and $\mathbf{R}$ fixed. Values are normalised against those achieved using optimal passive control (i.e. PTO spring stiffness and damping are optimised for each sea state without considering displacement limits) and results are shown for three PM sea-states. It is seen that low values of λ result in higher captured energy as the reactor motion is not heavily penalised in the cost function, and increasing λ has the desired effect of reducing the cyclic component of the mooring forces. Inevitably, increasing λ impacts negatively on captured power since the float velocity tracking error is less heavily penalised. Therefore, the operator may select a suitable trade-off based upon economic analysis.

To analyse the effects more closely, we now focus on the 10 s energy period sea state and present results comparing the optimal passive system performance against the AVT strategy

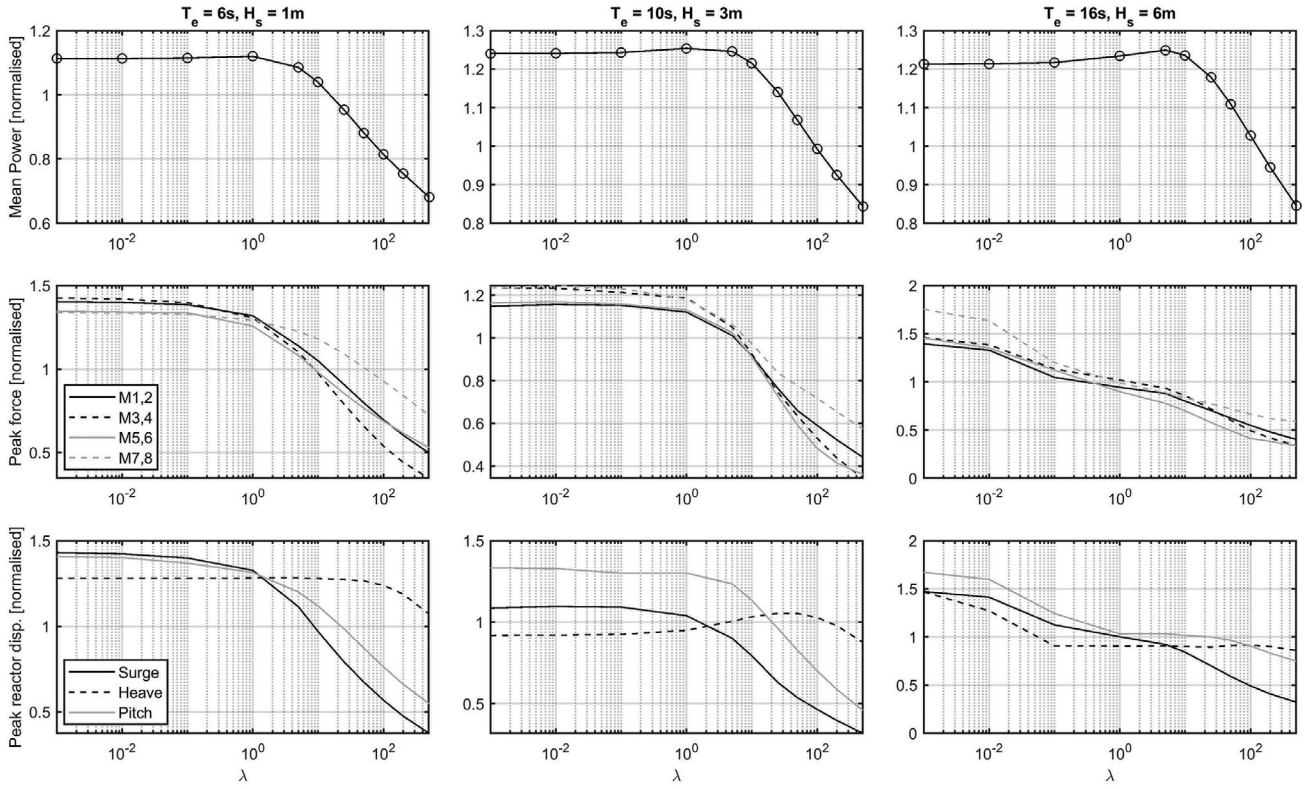

FIGURE 9 Variation of mean captured power (top row), peak mooring forces (middle row) and peak reactor displacement (bottom row) under optimal control for a range of λ. Values are normalised against the optimally tuned passive system.

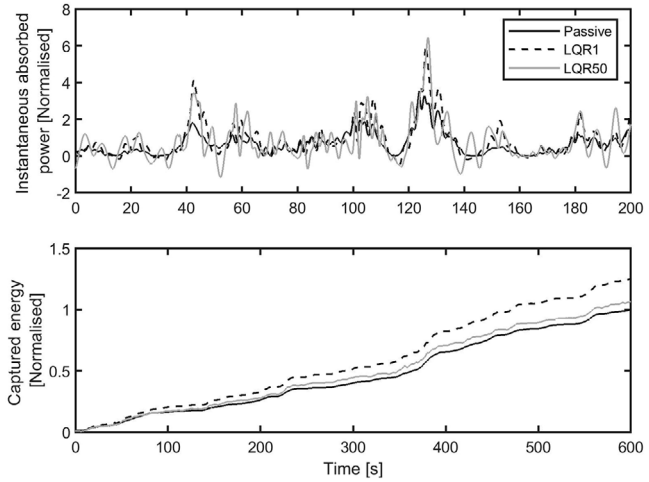

FIGURE 10 Instantaneous captured power and accumulated energy for passive and LQR controlled systems with $\lambda = 1, 50$. Values are normalised against the optimally tuned passive system.

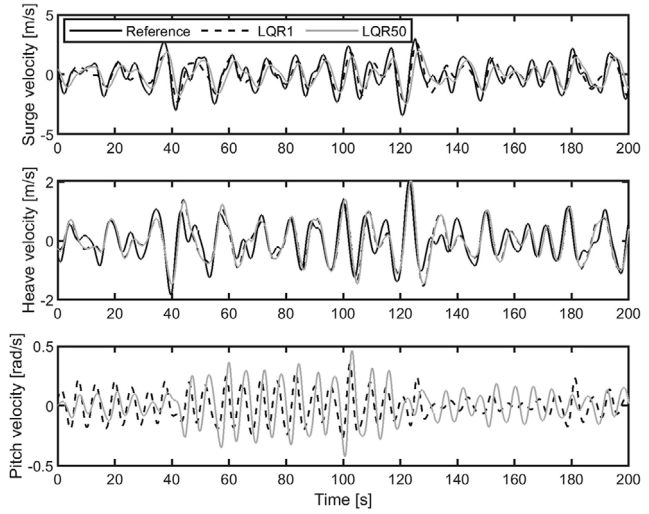

FIGURE 11 Velocity tracking of LQR systems with $\lambda = 1, 50$

with $\lambda = 1$ and with $\lambda = 50$. These tuning states are chosen as one gives good energy capture, whilst the other captures slightly more energy than the optimal passive system but significantly reduces mooring loads, particularly in high energy seas.

Figure 10 shows the instantaneous captured power and energy for the AVT controller with two tuning states compared with the passive system. As expected from Figure 9, we see a 25% increase in captured energy for $\lambda = 1$ and similar captured energy to the passive system for $\lambda = 50$. The disadvantage of such active control strategies is seen in the greater fluctuation of instantaneous power and the requirement for bi-directional power flow.

Figure 11 shows the float velocity tracking performance of the AVT. The optimal reference velocity is required to be tracked by the float to achieve good power capture. We see good tracking, though it is degraded compared to the controller used in [9] by using the PTO to also regulate reactor motion. Tracking

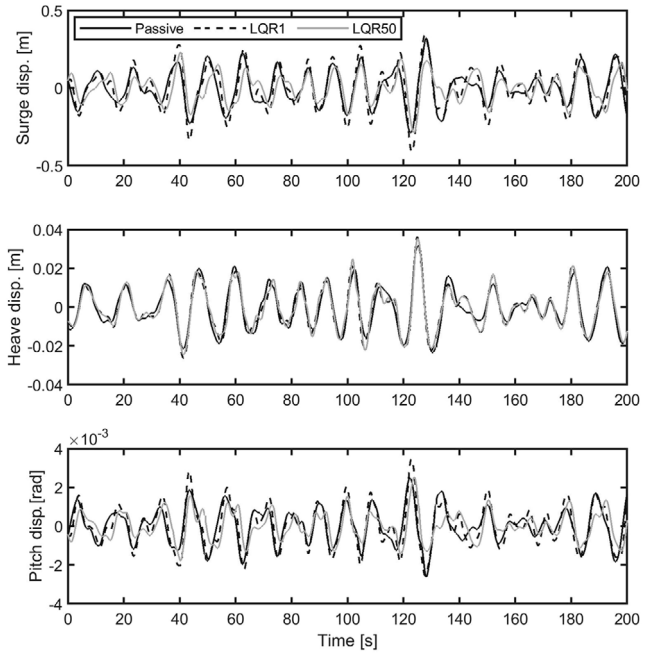

FIGURE 12 Reactor position for passive and LQR systems, $\lambda = 1, 50$

is only enforced in the surge and heave directions; pitch motion is included for completeness.

Reactor displacement $\mathbf{x}_R$ from its nominal position is shown in Figure 12. Substantial reduction of motion in the surge and pitch DOFs is clearly seen for $\lambda = 50$. The mooring system is very stiff in heave, so this is less affected.

Mooring line forces are shown in Figure 13. These are calculated according to equation 6. The pre-load is subtracted so only the cyclic component is shown. For head-on waves these act in pairs, so are displayed as such for clarity. Significant reduction of mooring line forces is seen for $\lambda = 50$, as expected from the reduced reactor motion. It is also interesting to examine the change in PTO forces as a result of the new control strategies. Figure 14 shows the cyclic PTO forces for the passive and AVT controlled systems. Again, for head-on waves the PTO lines act in pairs. We see an increase in PTO forces for lines 1 and 2 (which face the incoming waves) and a reduction in forces for lines 3 and 4 with $\lambda = 50$ so there could be further scope for design optimisation.

4.2 | Effect on fatigue loading

We now estimate the effects of applying the AVT strategy in terms of fatigue damage to the mooring and PTO lines. The following analysis is intended to be indicative only and not a comprehensive fatigue analysis. We follow the method presented in [17] and make the following common assumptions:

1. Miner's rule applies, i.e. the accumulated damage D in a line is given by

$$D = \sum_j \frac{n_j}{N_j} \tag{24}$$

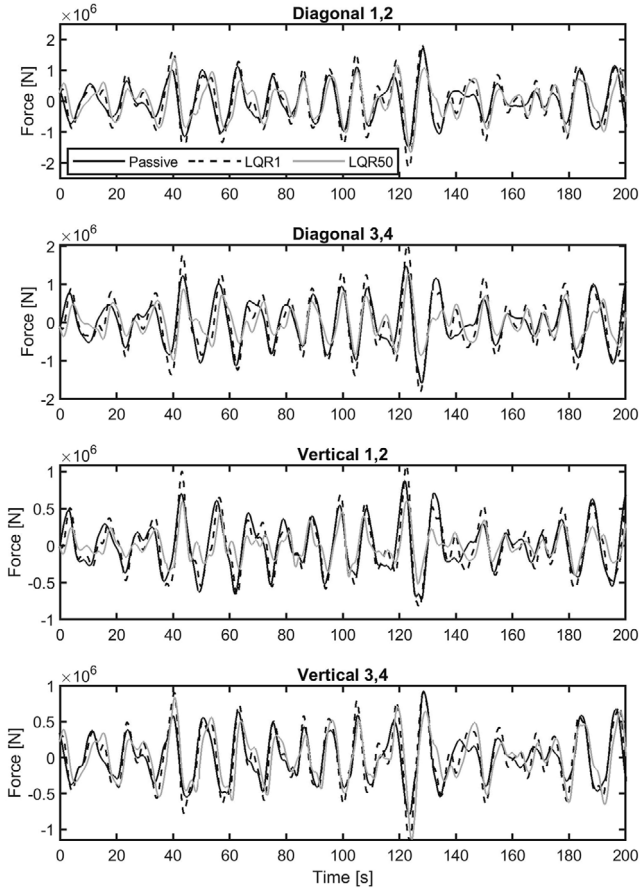

FIGURE 13 Cyclic component of mooring line forces with passive and LQR systems with $\lambda = 1, 50$

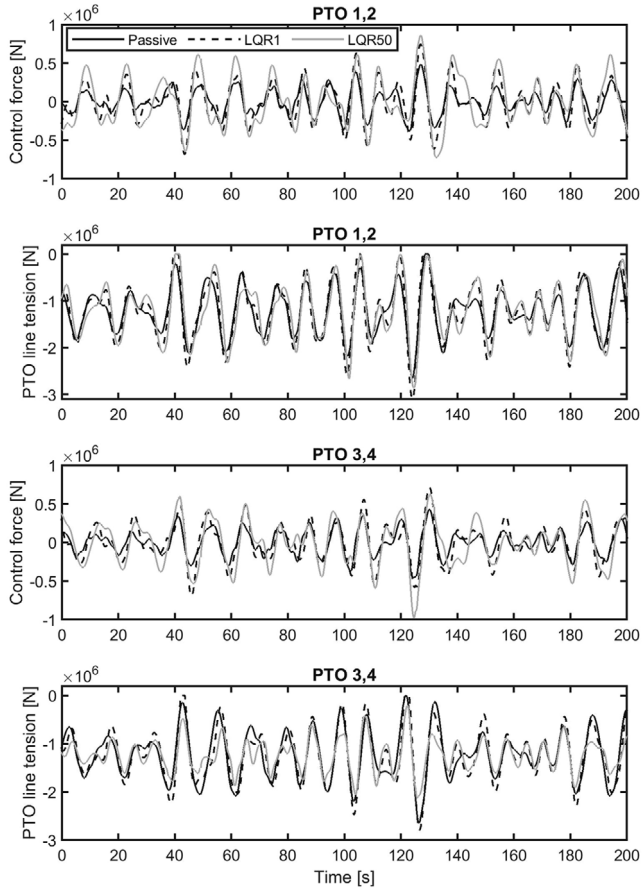

FIGURE 14 PTO line forces with passive and LQR systems with $\lambda = 1, 50$

where n_j is the number of cycles at stress state j and N_j is the number of cycles to failure at the same state.

2. Mean stress (pre-load) can be ignored, only the cyclic component is important.
3. The lines experience high cycle fatigue above any fatigue limit, therefore Basquin's model applies, i.e.

$$N_j = \frac{B}{S_j^m} \tag{25}$$

where S_j is the reversing stress (stress range) and B and m are material coefficients extracted from the linear section of the log-log SN curve.

Under these assumptions, accumulated damage can be expressed in terms of stress ranges as

$$D = \frac{1}{B}\sum_j n_j S_j^m \tag{26}$$

If two sets of cycles (1 and 2) are applied to the same PTO or mooring line, a relative accumulated damage index may be expressed as

$$R = \frac{D_1}{D_2} = \frac{\sum_i n_{1,i} S_{1,i}^m}{\sum_j n_{2,j} S_{2,j}^m} \tag{27}$$

Applying this method to all 8 mooring lines and 4 PTO lines, we can calculate the relative accumulated damage in the lines for the AVT controlled system compared to the passive system. Rainflow-counting is used to obtain load reversals from the tension time-series of a line.

By way of example, Figure 15 shows the load reversals and rainflow histograms for three load cases as experienced by diagonal mooring lines 1 and 2 over 700 s simulations. The cases are the PM spectrum with $T_e = 10$ s and $H_s = 3$ m with optimal passive damping and AVT control using $\lambda = 1, 50$. Figure 16 shows the results for the same load cases as experienced by diagonal mooring lines 3 and 4. The relative damage indices are given for all lines and for all three test sea-states in Table 2. These values assume the mooring lines to be made from wet nylon stranded rope ($m = 3.5$) [18] and the PTO lines to be made from steel stranded rope ($m = 4.0$) [17]. The $\lambda = 100$ case is included to demonstrate further reductions in mooring and PTO loads. With this value of λ (as shown in Figure 9), the

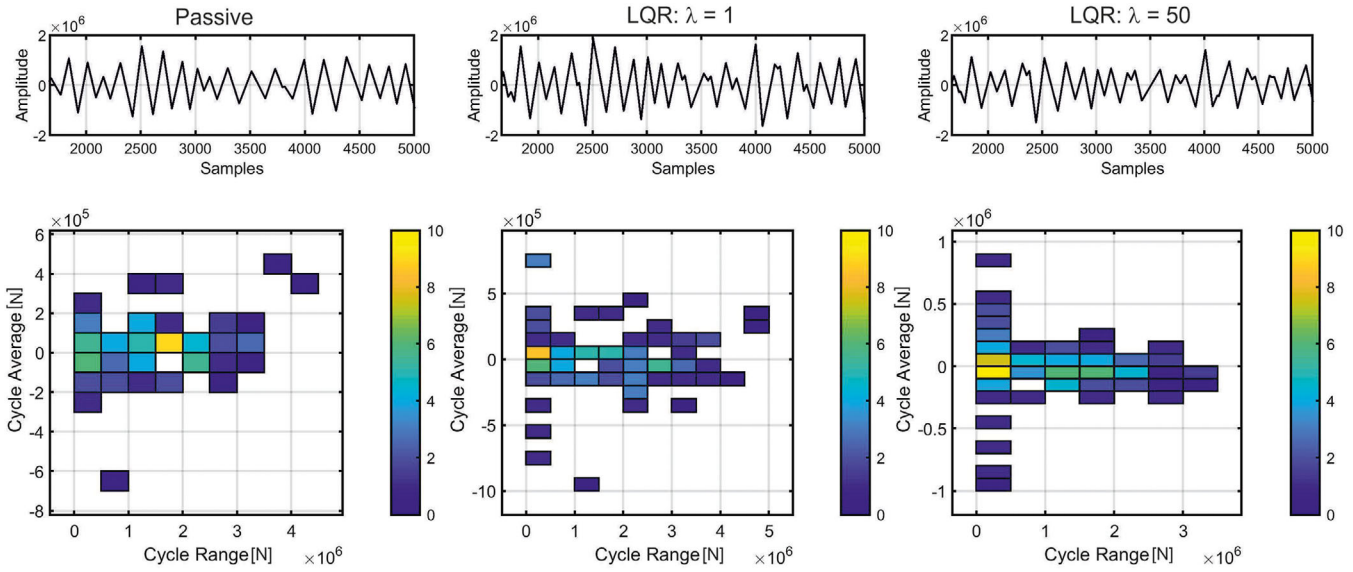

FIGURE 15 Load reversals and rainflow histograms for diagonal mooring lines 1 and 2 for passive and LQR controlled systems with $\lambda = 1, 50$ in PM spectrum with $T_e = 10$ s and $H_s = 3$ m

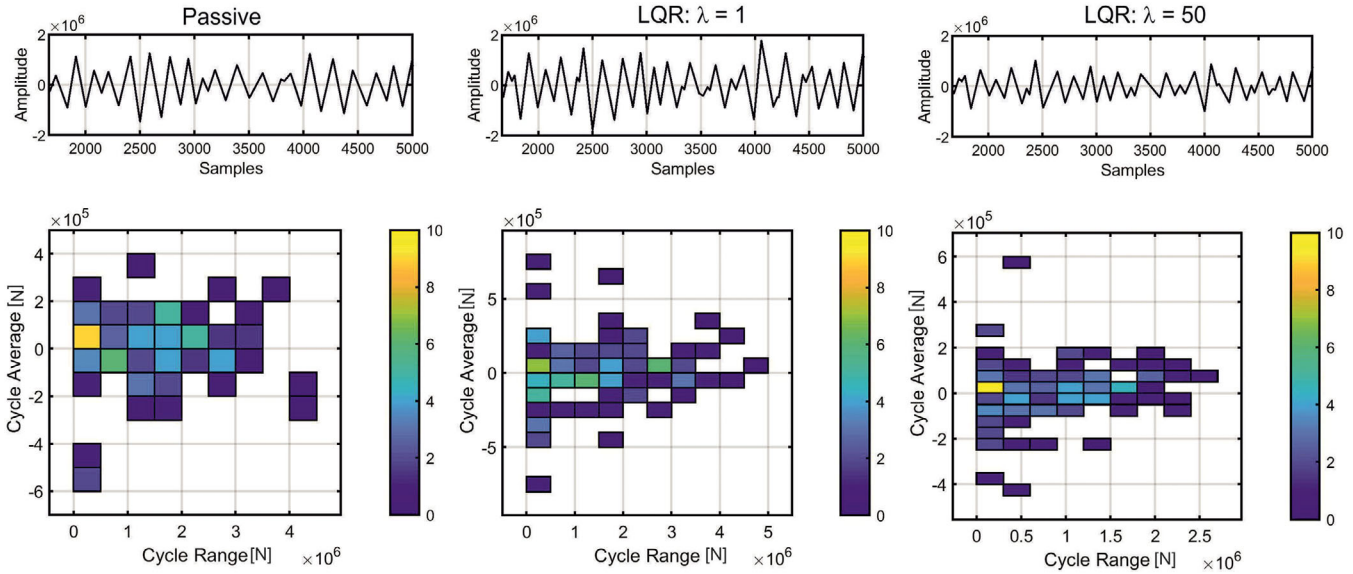

FIGURE 16 Load reversals and rainflow histograms for diagonal mooring lines 3 and 4 for passive and LQR controlled systems with $\lambda = 1, 50$ in PM spectrum with $T_e = 10$ s and $H_s = 3$ m

TABLE 2 Relative accumulated damage of mooring and PTO lines

	$H_s = 1$ m, $T_e = 6$ s			$H_s = 3$ m, $T_e = 10$ s			$H_s = 6$ m, $T_e = 16$ s		
Structural member	$\lambda = 1$	$\lambda = 50$	$\lambda = 100$	$\lambda = 1$	$\lambda = 50$	$\lambda = 100$	$\lambda = 1$	$\lambda = 50$	$\lambda = 100$
MD1,2	2.58	0.54	0.34	2.30	0.71	0.46	1.14	0.37	0.24
MD3,4	2.42	0.21	0.11	1.88	0.27	0.13	1.09	0.15	0.08
MV1,2	2.32	0.35	0.25	1.31	0.21	0.13	0.96	0.15	0.10
MV3,4	2.66	1.07	0.70	2.21	1.18	0.90	1.13	0.69	0.57
PTO1,2	3.08	1.97	1.61	2.27	2.12	1.74	1.30	1.23	1.08
PTO3,4	2.30	0.32	0.24	1.34	0.22	0.14	1.03	0.35	0.32

mean captured power is reduced to 80% of that when applying optimal damping in the lowest energy sea state. In the two higher energy sea-states, however, the captured power is the same as that for optimal damping while the accumulated damage in mooring lines is significantly reduced. It is readily achievable to vary λ depending on the sea state to suitably optimise performance.

4.3 | Summary discussion

The original objective of this study was to regulate reactor motion and reduce mooring loads and therefore fatigue damage in the mooring lines. It is demonstrated that, using this strategy, the WEC operator may choose λ to maximise economic return by trading power capture against accumulated damage in the mooring and PTO lines. For example, in the more common lower energy sea-states, a low value of λ could be used to maximise power capture. A value of $\lambda = 50$ is seen to still return good power capture while reducing accumulated damage in mooring lines by up to 79% (with a marginal increase in damage for vertical mooring lines 3 and 4).

In the highest energy sea-state it may be desirable to use a higher value of λ to limit peak mooring loads. A value of $\lambda = 100$ will capture the same power as the optimal passively damped system while reducing accumulated damage by between 43% and 92% for mooring lines. Accumulated damage is reduced by 68% for PTO lines 3 and 4 with a marginal increase in damage for lines 1 and 2.

5 | CONCLUSIONS

This study extends previous work on power-maximising control to investigate the potential of using PTO control to simultaneously capture power and reduce reactor motion and mooring line cyclic loading. These additional objectives are complimentary to power capture in terms of the overall cost of a WEC since reduced fatigue loading in mooring lines is clearly desirable. However, the objectives are competitive and can be suitably balanced by an appropriate PTO control strategy. Here we have utilised an AVT controller designed with an LQR method to enable differential penalising of system states. The resulting controller is easily tuned to adjust the trade-off between power capture and reactor motion, and therefore mooring cyclic loading.

The controller was applied to a comprehensive multi-body simulation of the multi-DOF WaveSub WEC. Three irregular sea-states covering the full range of operational conditions were applied and performance was compared against a benchmark optimally tuned passively damped system. It has been shown that the AVT controller may be tuned to capture the same mean power as an optimally tuned passively damped system over a 700s irregular sea state, while reducing reactor motion. It was shown that significant reduction of mooring line cyclic loading could be achieved. In the highest energy sea-state tested, accumulated damage in mooring lines was reduced by between 43% and 92%. The disadvantage is increased loading on wave-facing PTO lines and greater fluctuation of captured power. These are issues for all power-maximising control strategies, however.

Mismatch between the multi-body simulation and the linearised state-space model used to design the controller is inherent and the controller has been shown to be robust against this. However, the multi-body simulation is limited by having linearised BEM hydrodynamic coefficients comprising part of the system dynamics. In reality these coefficients will be nonlinear for large motions and complex geometries. Experimental validation using a scaled device is a subject for future investigation.

ORCID

A.J. Hillis https://orcid.org/0000-0002-7017-5709
C.R.P. Courtney https://orcid.org/0000-0002-6433-8110

REFERENCES

1. Harris, R.E., Johanning, L., Wolfram, J.: Mooring systems for wave energy converters: A review of design issues and choices. In: Proceedings of the Institution of Mechanical Engineers Part B Journal of Engineering Manufacture, pp. 180–189. The Institute of Marine Engineering, Science and Technology, London (2004)
2. Johanning, L., Smith, G.H., Wolfram, J.: Mooring design approach for wave energy converters. Proceedings of the Institution of Mechanical Engineers, Part M: Journal of Engineering for the Maritime Environment 220(4), 159–174 (2006)
3. Luxmoore, J.F., et al.: Analytical performance assessment of a novel active mooring system for load reduction in marine energy converters. Ocean Eng. 124, 215–225 (2016)
4. Wang, Y., et al.: Hydrodynamic response of a combined wind-wave marine energy structure. Journal of Marine Science and Engineering 8(4), 253 (2020)
5. Muliawan, M.J., Karimirad, M., Moan, T.: Dynamic response and power performance of a combined spar-type floating wind turbine and coaxial floating wave energy converter. Renewable Energy 50, 47–57 (2013)
6. Borg, M., Collu, M., Brennan, F.P.: Use of a wave energy converter as a motion suppression device for floating wind turbines. Energy Procedia 35, 223–233 (2013)
7. Genest, R., Ringwood, J.: A critical comparison of model-predictive and pseudospectral control for wave energy devices. Journal of Ocean Engineering and Marine Energy 2(4), 485–499 (2016)
8. Fusco, F., Ringwood, J.V.: A simple and effective real-time controller for wave energy converters. IEEE Trans. Sustainable Energy 4(1), 21–30 (2013)
9. Hillis, A.J., et al.: Active control for multi-degree-of-freedom wave energy converters with load limiting. Renewable Energy 159, 1177–1187 (2020)
10. Hillis, A.J., et al.: Model predictive control of a multi-degree-of-freedom wave energy converter with model mismatch and prediction errors. Ocean Eng. 212, 107724 (2020)
11. Yu, Y., et al.: Development and demonstration of the WEC-Sim wave energy converter simulation tool. In: Proceedings of the 2nd Marine Energy Technology Symposium, pp. 1–8. US Department of Energy, Washington, DC (2014)
12. Babarit, A., Delhommeau, G.: Theoretical and numerical aspects of the open source BEM solver NEMOH. Paper presented at Proceedings of the 11th European Wave and Tidal Energy Conference, Nantes, 6–11 Sept 2015
13. Cummins, W.E.: The Impulse Response Function and Ship Motions. Schiffstechnik 9, 101–109 (1962)
14. Faraggiana, E., et al.: Computational modelling and experimental tank testing of the multi float WaveSub under regular wave forcing. Renewable Energy 152, 892–909 (2020)
15. Scruggs, J.T., et al.: Optimal causal control of a wave energy converter in a random sea. Appl. Ocean Res. 42, 1–15 (2013)

16. Hillis, A.J., Brask, A., Whitlam, C.: Real-time wave excitation force estimation for an experimental multi-DOF WEC. Ocean Eng. 213, 107788 (2020)
17. DNV-GL.: DNVGL-OS-E301–Position Mooring. Offshore Standard (2018) https://rules.dnv.com/docs/pdf/DNV/os/2018-07/dnvgl-os-e301.pdf, July 2018
18. Weller, S.D., et al.: Synthetic mooring ropes for marine renewable energy applications. Renewable Energy 83, 1268–1278 (2015)

How to cite this article: Hillis, A.J., Courtney, C.R.P., Brask, A.: Wave energy converter platform stabilisation and mooring load reduction through power take-off control. IET Renew. Power Gener. 15, 3243–3254 (2021). https://doi.org/10.1049/rpg2.12242